Near-field spatial imaging of a Ni-like Ag 140-Å x-ray laser

J. Nilsen,[1] J. Zhang,[2] A. G. MacPhee,[3] J. Lin,[4] T. W. Barbee, Jr.,[1] C. Danson,[5] L. B. Da Silva,[1] M. H. Key,[1] C. L. S. Lewis,[3] D. Neely,[5] R. M. N. O'Rourke,[3] G. J. Pert,[6] R. Smith,[4] G. J. Tallents,[4] J. S. Wark,[2] and E. Wolfrum[2]

[1]*Lawrence Livermore National Laboratory, Livermore, California 94550*

[2]*Clarendon Laboratory, Department of Physics, University of Oxford, Oxford OX1 3PU, United Kingdom*

[3]*School of Mathematics and Physics, Queens University of Belfast, Belfast BT7 1NN, United Kingdom*

[4]*Department of Physics, University of Essex, Colchester CO4 3SQ, United Kingdom*

[5]*Central Laser Facility, Rutherford Appleton Laboratory, Chilton, Oxon OX11 0QX, United Kingdom*

[6]*Department of Computational Physics, University of York, York YO1 5DD, United Kingdom*

(Received 7 May 1997)

We measure the two-dimensional, near-field spatial distribution of a 140-Å nickel-like silver x-ray laser at the output aperture with high magnification using a curved multilayer x-ray mirror to image the output onto an x-ray charge-coupled device camera. Lasing is created by illuminating silver slab targets with a pair of 75 ps laser pulses separated by 2.2 nsec from the Vulcan laser. The two-dimensional, high-resolution, spatial image shows the x-ray laser source size and its position relative to the target surface. A dramatic change in both the position and source size are observed for the refraction compensating curved target as compared with the flat targets. [S1050-2947(97)02310-X]

PACS number(s): 42.55.Vc, 42.60.Jf, 52.70.La, 32.30.Rj

I. INTRODUCTION

Over the last several years the multiple pulse technique has been used with great success to create strong lasing in many neonlike ions on the $3p\ ^1S_0 \rightarrow 3s\ ^1P_1$ laser transition [1]. This technique has also been used quite successfully with the lanthanides to produce strong lasing on the nickel-like $3d^9\,4d(J=0) \rightarrow 3d^9\,4p(J=1)$ laser transitions [2–4]. While this technique opened the door to lasing in these nickel-like ions using slab targets, lasing was still far below saturation. By optimizing the pulse separation and contrast and moving to lower Z, recent experiments using silver slab targets have observed saturated laser output, with an laser output of 90 μJ, on the nickel-like silver $3d^9\,4d(J=0) \rightarrow 3d^9\,4p(J=1)$ laser transition at 140 Å [5]. Using this bright silver laser, we measure the near field, two-dimensional distribution of the output of the nickel-like silver 140-Å laser to characterize the source size and its position relative to the target surface. The position of the lasing relative to the target surface provides valuable information to compare with computer simulations so that we can understand the plasma conditions under which lasing occurs and how to improve these laser systems. Other recent papers have looked at near field [6–8] or far field [9] images of the neonlike germanium 196-Å $3p\ ^1S_0 \rightarrow 3s\ ^1P_1$ laser transition using the various multiple pulse techniques but nickel-like lasers have never been imaged before because of their low intensity and short wavelength.

II. EXPERIMENTAL SETUP

The experimental setup is shown in Fig. 1 and consists of two slab targets which are coupled lengthwise and illuminated in opposite directions. Six beams of the 1.05-μm Vulcan Nd:glass laser with a 75 ps duration were used in a standard off-axis focus geometry. The $f/2.5$ spherical lenses focus three beams from one side of the target chamber to a spot focus which is then imaged by $f/2.5$ off-axis spherical mirrors to produce a line focus 2.5-cm long by 200-μm wide. The total energy on each target is about 75 J after 30% losses for reflection and transportation by the relay and focusing system, giving an irradiance of 20 TW/cm^2 on target. The other three beams are 180° opposed in a second line focus which illuminates the second slab target and produces a plasma with a density gradient in the opposite direction which helps compensate for the refraction of the x-ray laser beam from the first plasma.

The prepulse was produced by splitting the oscillator pulse into two pulses before the preamplifiers in the Vulcan laser. A prepulse with 15–20% of the total energy on target was produced and delivered 2.2 ns in advance of the main

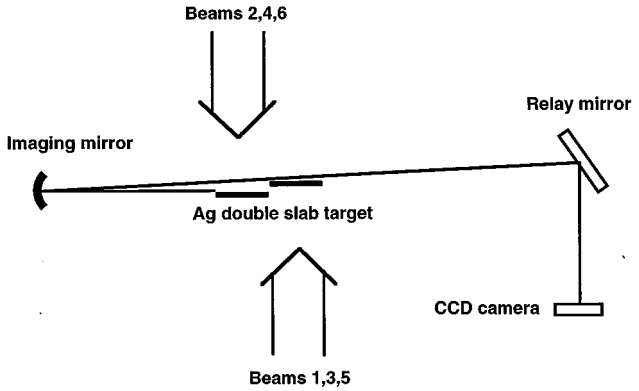

FIG. 1. Schematic of the experimental setup showing the Vulcan beams illuminating the double slab silver targets. The output aperture of the 140-Å nickel-like silver laser is imaged with magnification 22.1 on to the CCD camera using a curved multilayer mirror with 25 cm focal length. A flat multilayer mirror relays the image and helps to eliminate background. The setup is not shown to scale.

pulse. The prepulse level and pulse duration were monitored by a fast photodiode.

Flat slab targets used in the experiment were 1.8-cm long, 200-μm wide, silver stripes coated on glass substrates. Both ends of the slab target were placed well within the line focus to avoid cold plasmas at the ends of the targets. The two slab targets were aligned so that they were parallel with an adjustable separation (in the direction perpendicular to the target surfaces) between the surface planes and an axial separation of 500 μm between the two targets. For some shots, curved targets with a 100-cm radius of curvature were used to make a comparison with the performance of the flat slab targets. The curved targets were made by diamond machining a copper substrate which was then coated with 1 μm of silver.

Since the x-ray laser pulse duration is comparable to the propagation time, traveling wave excitation for the two successive targets is necessary to achieve sufficient amplification. The three drive beams (1,3,5) for the first slab target were therefore timed 60 ps earlier than the three beams (2,4,6) for the second target. The targets were aligned relative to the target chamber axis to accuracies of ± 1 mrad and ± 3 μm.

The two-dimensional (2D), high-resolution, spatial imaging diagnostic consisted of a 2.5-cm diameter, 50-cm radius of curvature molybdenum/silicon multilayer mirror placed 26.1 cm from the output end of the silver laser at near normal incidence. The multilayer mirror consisted of 60 layer pairs with a spacing of 72.3 Å which gave the mirror a peak reflectivity of approximately 65% and a full-width at half-maximum (FWHM) bandwidth of 6 Å for 140 Å radiation at normal incidence. This mirror images the output aperture of the 140-Å nickel-like silver laser onto an IntraSpec IV back-thinned x-ray charge-coupled device (CCD) camera which was placed 575 cm from the mirror. A flat, 5-cm diameter, molybdenum/silicon multilayer mirror was placed 350 cm from the imaging mirror to relay the image onto the CCD camera and to filter out background radiation from the plasma. The second mirror used sixteen layer pairs with 105 Å spacing for the 45° angle of incidence and had peak reflectivity of approximately 35% and a bandwidth of 15 Å. Figure 2 shows the reflectivity of the two mirrors as well as the total reflectivity of the combined system. The total reflectivity peak at 22% with a bandwidth of 6 Å. The reflectivities are calculated based on the system parameters but the central bandpass and bandwidth are verified experimentally and the peak measured reflectivity is approximately 90% of the calculated value. The 45° relay mirror does act as a polarizer but the reflectivity curve for the flat mirror is averaged assuming an unpolarized x-ray laser beam. A 55-μg/cm^2 (2000-Å) thick aluminum filter was used in front of the relay mirror to eliminate optical light and a 50-μg/cm^2 (2200-Å) thick carbon filter was used in front of the imaging mirror to attenuate the signal, eliminate shorter and longer wavelength radiation, and help protect the mirror. Even though the aluminum edge is at 170 Å it was critical to use the aluminum filter to eliminate optical light. We did try a silicon filter, which has an ideal edge at 125 Å, but this was transparent to the optical light as was the carbon filter used. The CCD consisted of a 1024 by 1024 array of 24 μm pixels which recorded 16 bits of data per pixel. At 140 Å the CCD produced 2 counts per photon. The magnification was 22.1, resulting in spatial resolution of approximately 1 μm.

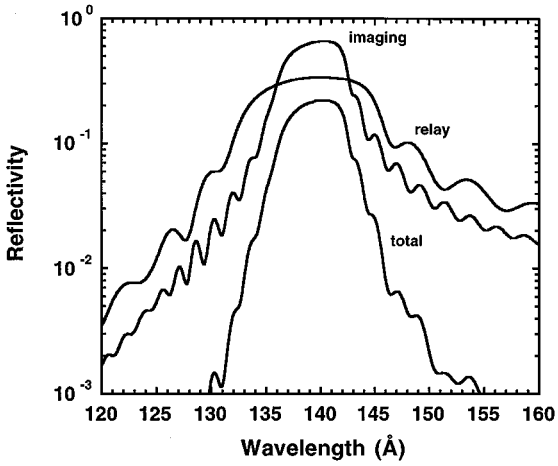

FIG. 2. Individual and combined reflectivity of the two molybdenum/silicon multilayer mirrors (imaging and relay) versus wavelength. The total reflectivity of the combined system peaks at 22% with a bandwidth of 6 Å.

From our time-resolved spectral data we know that lasing occurs only during the second illumination pulse with typical durations of 30–50 ps so the laser itself acts as the strobe to enable the CCD camera to take a snapshot of the plasma. The actual CCD acquisition time was 1 msec. Figure 3 shows a typical spectrum of the silver laser for a single curved target as seen by a flat field spectrometer. The nickel-like silver laser is monochromatic and the laser line at 140 Å completely dominates the background. The silicon edge from the CCD camera used to record the spectrum can be seen at 125 Å. This is the same CCD camera used in the imaging diagnostic described above. It is this combination of a bright laser line with the use of multilayer mirrors which allows us to image the laser output from the nickel-like laser. Previously, most nickel-like lasers were weak and their wavelengths were much shorter where multilayer mirrors work poorly, if at all. By moving to the long wavelength side of

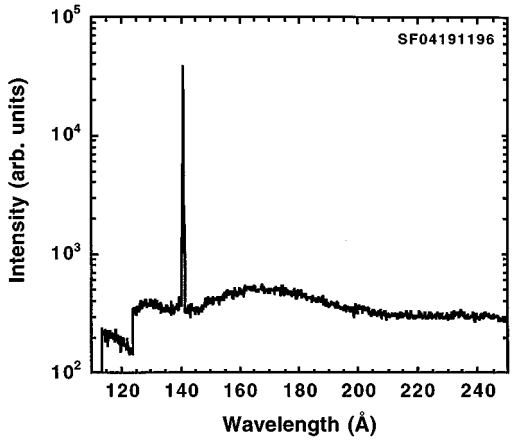

FIG. 3. Intensity versus wavelength of the output of a typical nickel-like silver laser showing the monochromatic laser output from the $4d \rightarrow 4p$ laser transition at 140 Å. The target was a single 1.8-cm long curved target with 100-cm radius of curvature.

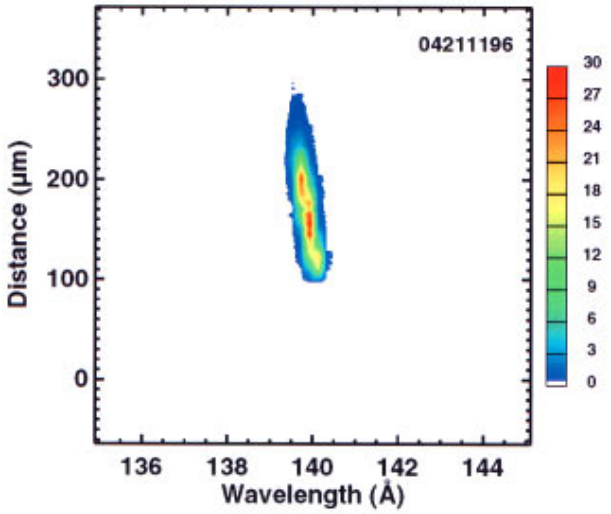

FIG. 4. (Color) Image of a single 1.8-cm long flat silver slab target observed using a flat field spectrometer in the image plane to verify the performance of the two-dimensional imaging diagnostic. The 140-Å laser emission completely dominates the image. The main plasma expansion is in the vertical direction. The color bar shows the intensity in 100's of CCD counts.

the 125 Å silicon edge, we can use the very efficient molybdenum/silicon multilayer mirrors. One problem we encountered in some of our early experiments was large backgrounds from optical light which swamped the signal from the x-ray laser. This was due to optical transmission through our filters and was fixed by using the thin aluminum filter.

To check the transmission of our imaging system, we temporarily put a flat field spectrometer in place of the CCD in the image plane to verify that the signal was indeed dominated by the 140-Å lasing from nickel-like silver. Figure 4 shows the image from the spectrometer for a single 1.8-cm long flat silver target. The spectrometer data was recorded using a smaller EEV series 15-11 back-thinned x-ray CCD which had an 256 by 1024 array of 27-μm pixels with the narrow axis in the dispersion direction. The dispersion was approximately 0.2 Å per pixel which gave a coverage of 50 Å around the laser line even though we only show the central 10 Å wide region in this figure. The vertical axis is the expansion direction of the plasma perpendicular to the target surface. The exact position of the target surface is not known because the background emission is too weak to locate the surface. The image is dominated by the 140-Å silver laser line and the white background seen in the image is more than 1000 times lower intensity than the laser line and has no spatial structure associated with it. In fact the laser line is only one pixel wide and a slight tilt can been seen in the data due to the axis of the CCD not being exactly aligned with the dispersion direction. This image verifies that our imaging setup is working properly and that the two-dimensional images described in the next section are images of the 140-Å nickel-like silver laser line.

III. EXPERIMENTAL RESULTS AND CONCLUSIONS

We did a series of experiments to measure the near field output of the silver laser as we changed the target configuration. As shown in Fig. 5, we first varied the transverse

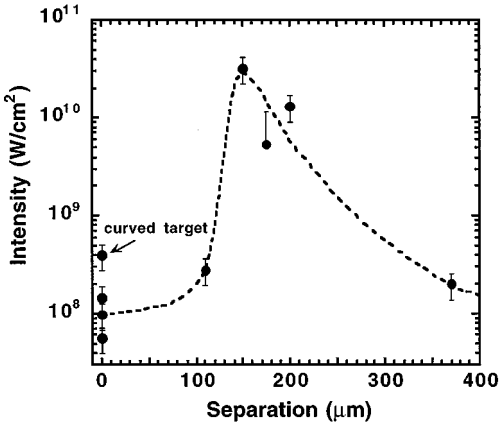

FIG. 5. Output intensity of the 140-Å nickel-like silver laser versus the perpendicular separation between the two opposing 1.8-cm long slab targets. Zero separation corresponds to a single 1.8-cm long slab target.

separation between the two slab lasers to determine that the coupling was optimized for a separation of about 150 μm. Figure 6 shows the two-dimensional spatial image for the optimum 150-μm separation. For this shot we used a thicker 100-μg/cm^2 carbon filter in front of the imaging mirror to avoid saturating the CCD camera. We measured a source size of 43 by 57 μm^2 and a total x-ray laser energy of 90 μJ [5]. The target surface is at zero in the vertical direction and the plasma is expanding in the positive vertical direction. The position of the target surface is determined by locating the abrupt change in the background radiation. We estimate the uncertainty in the target surface as ± 10 μm. The horizontal direction is parallel with the target surface and to the narrow dimension (200-μm wide) of the line focus of the Vulcan laser. Using the imaging diagnostic to study the sensitivity of the output to the separation between the slabs offers the big advantage of being able to measure the total two-dimensional output of the laser; i.e., all the beam is col-

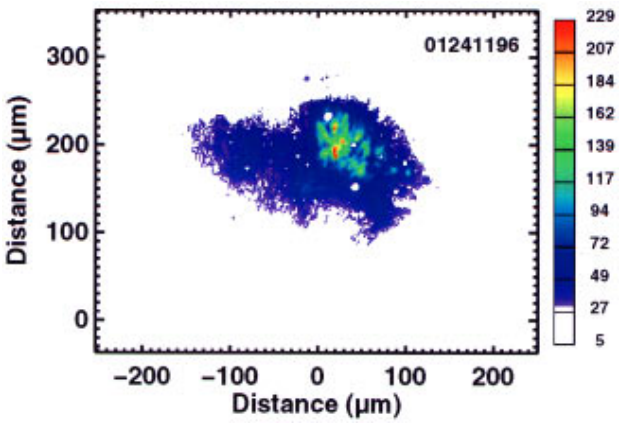

FIG. 6. (Color) Spatial image of the 140-Å laser emission at the output aperture of the double flat slab target with optimum separation of 150 μm. Each slab was 1.8-cm long. The target surface is at zero on the vertical axis with the plasma expanding upwards. This shot used a thicker 100 μg/cm^2 carbon filter in front of the imaging mirror to avoid saturating the CCD camera. The color bar shows the intensity in 100's of CCD counts.

lected compared to the sample that a spectrometer with a slit would collect.

We also measured the source size and position relative to the target surface for a variety of target configurations. Figure 7 shows typical data which compares the output of a single slab target, a double slab target, and a single curved target. First let us compare the single and double slab targets. The double slab target shown here has a 175-μm separation, which is slightly more than optimum, but which uses the same 50-μg/cm^2 carbon filter and was done consecutively with the single slab target. The most intense laser region in both cases is 100–200 μm from the target surface with the double slab target much brighter. The color scale is given to the right of each figure with red being the highest intensity. A logarithmic scaling of the colors was used to bring out the weak features. The intensity on the color bar is given in 100's of CCD counts and is different for each target. The lasing from the double slab target is closer to the surface than that for the single slab target and is slightly saturated, which tends to increase the apparent source size for this particular image. For the single slab target the lasing peaks about 160 μm from the target surface with a source size about 120-μm wide in the line focus transverse direction and 40-μm wide in the plasma expansion direction.

If we now look at the single curved target, Fig. 7(c), there is a dramatic difference between this target and the two flat targets. For the curved target the lasing region is much closer to the surface, has a very different shape, and is brighter than the single flat target. As a reminder, both the single flat and curved targets are the same 1.8-cm length and the target surface is defined at the output aperture of the x-ray laser. In typical laser produced plasmas used to make x-ray lasers, the electron density of the plasma decreases as you go further from the target surface. Since the index of refraction of the plasma at the x-ray laser wavelength is proportional to one minus a constant times the electron density, the gradient in the electron density results in a gradient in the index of refraction, but with opposite sign. This tends to make the x rays propagating through the gain region bend toward the lower density, lower gain region which is further from the target surface. By using a curved target one can try to bend the target surface in the same direction as the propagating x ray to keep the x rays in the gain region for a longer distance. A discussion of curved targets and refraction issues can be found in Refs. [8–11]. The curvature is a static correction for one given value of the gradient while the gradient in the plasma varies in time and space. However Fig. 7(c) does show the dramatic improvement possible with the curved target and suggests that a parameter study with different curvatures to optimize the single slab output would be very useful.

In conclusion, we present high-resolution, two-dimensional, spatial images at the output aperture of the 140-Å nickel-like silver laser which operates near saturation. From these images we can characterize the source size of the laser and its position relative to the target surface. By comparing the output from flat versus curved targets we can see the dramatic improvement which is possible due to the refraction compensation of the curved target. By comparing this data with computer simulation we can try to improve our

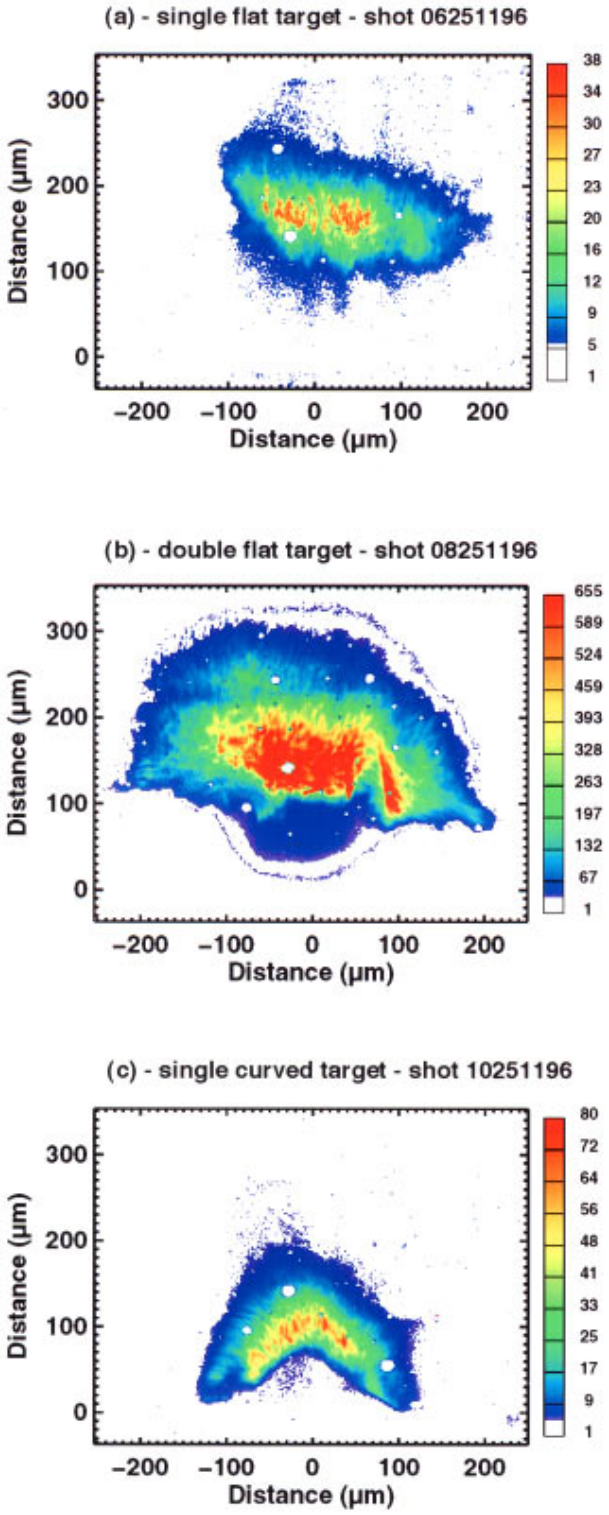

FIG. 7. (Color) Spatial image of the 140-Å laser emission at the output aperture of three different silver targets. Target (a) is a single flat slab target, (b) is a double flat slab target with perpendicular separation of 175 μm, and (c) is a single curved target with 100 cm radius of curvature. Each slab was 1.8-cm long. The target surface is at zero on the vertical axis with the plasma expanding upwards. The color bar shows the intensity in 100's of CCD counts.

modeling capability and ability to design even more efficient nickel-like x-ray lasers.

ACKNOWLEDGMENTS

The authors would like to thank the Vulcan laser operations, the target preparation and engineering groups of the Central Laser Facility, and H. Louis and A. Demiris of LLNL for their help and cooperation. The work of the LLNL authors was performed under the auspices of the U.S. Department of Energy by the Lawrence Livermore National Laboratory under Contract No. W-7405-Eng-48. The work of the U.K. authors was performed with funding from the Engineering and Physical Research Council (EPSRC) under Grant Nos. GR/L11946, GR/L11809, GR/L11540, and GR/L11779.

[1] *X-ray Lasers 1996*, edited by S. Svanberg and C-G Wahlström, IOP Conf. Proc. No. 151 (Institute of Physics Publishing, Bristol, 1996), pp. 1–547.

[2] H. Daido, Y. Kato, K. Murai, S. Ninomiya, R. Kodama, G. Yuan, Y. Oshikane, M. Takagi, H. Takabe, and F. Koike, Phys. Rev. Lett. **75**, 1074 (1995).

[3] J. Nilsen and J. C. Moreno, Opt. Lett. **20**, 1386 (1995).

[4] H. Daido, S. Ninomiya, T. Imani, R. Kodama, M. Takagi, Y. Kato, K. Murai, J. Zhang, Y. You, and Y. Gu, Opt. Lett. **21**, 958 (1996).

[5] J. Zhang, A. G. MacPhee, J. Nilsen, J. Lin, T. W. Barbee, Jr., C. Danson, M. H. Key, C. L. S. Lewis, D. Neely, R. M. N. O'Rourke, G. J. Pert, R. Smith, G. J. Tallents, J. S. Wark, and E. Wolfrum, Phys. Rev. Lett. **78**, 3856 (1997).

[6] J. C. Moreno, J. Nilsen, Y. L. Li, P. X. Lu, and E. E. Fill, Opt. Lett. **21**, 866 (1996).

[7] J. Zhang, J. Warwick, E. Wolfrum, M. H. Key, C. Danson, A. Demir, S. Healy, D. H. Kalantar, N. S. Kim, C. L. S. Lewis, J. Lin, A. G. MacPhee, D. Neely, J. Nilsen, G. J. Pert, R. Smith, G. J. Tallents, and J. S. Wark, Phys. Rev. A **54**, 4653 (1996).

[8] J. Nilsen, J. C. Moreno, L. B. Da Silva, and T. W. Barbee, Jr., Phys. Rev. A **55**, 827 (1997).

[9] G. Yuan, K. Murai, H. Daido, R. Kodama, and Y. Kato, Phys. Rev. A **52**, 4861 (1995).

[10] J. Nilsen, Y. L. Li, P. X. Lu, J. C. Moreno, and E. E. Fill, Opt. Commun. **124**, 287 (1996); **124**, 415 (1996).

[11] R. Kodama, D. Neely, Y. Kato, H. Daido, K. Murai, G. Yuan, A. MacPhee, and C. L. S. Lewis, Phys. Rev. Lett. **73**, 3215 (1994).